Spatio-chromatic sensitivity explained by post-receptoral contrast

Spatio-chromatic sensitivity explained by post-receptoral contrast

Marcel Lucassen Philips Lighting Research, Eindhoven, The Netherlands

Marc Lambooij Philips Lighting Research, Eindhoven, The Netherlands

Dragan Sekulovski Philips Lighting Research, Eindhoven, The Netherlands

Ingrid Vogels Human-Technology Interaction, Eindhoven University of Technology, Eindhoven, The Netherlands

We measured and modeled visibility thresholds of spatial chromatic sine-wave gratings at isoluminance. In two experiments we manipulated the base color, direction of chromatic modulation, spatial frequency, the number of cycles in the grating, and grating orientation. In Experiment 1 (18 participants) we studied four chromatic modulation directions around three base colors, for spatial frequencies 0.15–5 cycles/deg. Results show that the location, size and orientation of fitted ellipses through the observer-averaged thresholds varied with spatial frequency and base color. As expected, visibility threshold decreased with decreasing spatial frequency, except for the lowest spatial frequency, for which the number of cycles was only three. In Experiment 2 (27 participants) we investigated the effect of the number of cycles at spatial frequencies down to 0.025 cycles/deg. This showed that the threshold elevation at 0.15 cycles/deg in Experiment 1 was at least partly explained by the small number of cycles. We developed two types of chromatic detection models and fitted these to the threshold data. Both models incorporate probability summation across spatially weighted chromatic contrast signals, but differ in the stage at which the contrast signal is calculated. In one, chromatic contrast is determined at the cone receptor level, the dominant procedure in literature. In the other model, it is determined at a postreceptoral level, that is, after cone signals have been transformed into chromatic-opponent channels. We applied Akaike's Information Criterion to compare the performance of the models and calculated their relative probabilities and evidence ratios. We found evidence in favor of the second model and conclude that postreceptoral contrast is the most accurate determinant for chromatic contrast sensitivity.

Introduction

Human color vision involves processing of both spatial and temporal information, retrieved from sampling of the retinal image by L, M, and S photoreceptor arrays having partly overlapping spectral sensitivities. This paper is concerned with spatial processing of (static) chromatic information only. It is generally accepted that three channels can be distinguished, one achromatic, dealing with intensity (luminance) information only, and two chromatically opponent pathways (red-green and yellow-blue). Their spatial sensitivities can be described by the contrast sensitivity function (CSF), which shows the sensitivity to contrast signals as a function of spatial frequency. Usually, sine-wave gratings are used to measure the contrast sensitivity at a particular spatial frequency. The achromatic CSF has a band-pass characteristic whose peak sensitivity (between 1 and 10 cycles/deg) shifts to higher spatial frequencies with increasing luminance (Campbell & Robson, 1968; Van Meeteren & Vos, 1972) and to lower frequencies with increasing viewing angle (Carlson, 1982). Rovamo, Luntinen, O., and Näsänen (1993), Barten (1999), Watson (2000), and Wuerger, Watson, and Ahumada (2002) provide models of the achromatic CSF.

Most studies have found that the shape of the chromatic CSF is low-pass with respect to spatial frequency. Since there are two chromatic channels,

Citation: Lucassen, M., Lambooij, M., Sekulovski, D., & Vogels, I. (2018). Spatio-chromatic sensitivity explained by post-receptoral contrast. *Journal of Vision*, *18*(5):13, 1–18, https://doi.org/10.1167/18.5.13.

https://doi.org/10.1167/18.5.13 Received November 24, 2017; published May 22, 2018 ISSN 1534-7362

Authors (year)	No. of base colors	No. of color directions	Luminance / retinal illuminance	Individualized isoluminance	Spatial frequency range (cycles/deg)	No. of participants	Orientation H = horizontal V = vertical D = diagonal	Field size (degrees)
Van der Horst & Bouman (1969)	1 (white) 1 (yellow)	2 1	0.3–160 td 1.6–220 td	Yes	0.7–18	1	Unclear	0.3 × 2.8
Granger & Heurtley (1973)	1	1	27 cd/m^2	Yes	0.125–1.25 0.7–20	2 6	V	12 × 8 3 × 2.5
Mullen (1985)	1 (R-G) 1 (Y-B)	1 1	15 cd/m^2 2.1 cd/m^2	Yes	0.1–5.3 0.06–6	2	H	2.2–23.5
Webster et al. (1990)	1	2	27.4 cd/m^2	Yes	0.5–4	2	H	9
Mullen (1991)	1	1	42 cd/m^2	Yes	0.24–3.2	1	H	Dependent on number of cycles and spatial frequency
Rajala et al. (1992)	4	2	5–20 cd/m^2	No	0.5–20	6	H/V/D	2
Owens et al. (2002)	17	4	5–35 cd/m^2	Yes	2.5–29.1	5	H	8 × 11
Wuerger et al. (2002)	1	2	40 cd/m^2	No	1.12–11.3	3	V	2 × 2
Kim et al. (2013)	1	2	0.02–200 cd/m^2	No	0.25–8	6	V	σ in Gaussian = 1.5 or 3
Vogels & Lambooij (2014)	3	4	108 cd/m^2	No	0.15–5	18	H/V	18.9

Table 1. Summary of studies reporting on chromatic contrast sensitivity at isoluminance, using static sine-wave gratings.

there are also two CSFs involved, usually measured along the red-green and yellow-blue direction. The red-green CSF has higher sensitivity and thereby reaches out to higher spatial frequencies. In Table 1 we provide a summary of the studies (in chronological order of publication) that have measured the static chromatic CSF with sine-wave gratings at fixed luminance or brightness. The table shows the authors and year of publication, the number of base colors (adapting colors), the number of chromatic directions around the base color, the luminance (range) or retinal illuminance, if individual isoluminance points were used, the spatial frequency range, the number of participants, the orientation of the sine-waves, and the visual field size. Besides chromatic contrast sensitivity, Wuerger et al. (2002) and Kim, Mantiuk, and Lee (2013) also measured mixtures of achromatic and chromatic sensitivity, leading to a mixed shape of the CSF, but those parts are not reported in the table. Owens, Westland, Van de Velde, Delabastita, and Jung (2002) used the largest number of adapting base colors (around the white point) and showed that the low-pass characteristic of the CSF is maintained, albeit for relatively high spatial frequencies (>2.5 cycles/deg). In the studies by Rajala, Trussell, and Krishnakumar (1992), Owens et al. (2002), and Kim et al. (2013), different luminance levels are used. The Kim et al. (2013) study shows how the sensitivity to chromatic contrast increases for increasing luminance levels, and stabilizes between 40 and 200 cd/m^2. As mentioned above, we only report studies or parts of studies in the table that concern static sine-waves.

As the table shows, the experimental settings are quite different, not to mention the differences in psychophysical techniques and procedures for measuring threshold. Except for the studies of Rajala et al. (1992), Wuerger et al. (2002), Kim et al. (2013), and Vogels and Lambooij (2014), individual isoluminance points were used to present stimuli at fixed brightness. Generally, a fairly low number of participants are used (1–6), which is not uncommon in psychophysical studies, but limits the applicability of results as they cannot be considered as a reliable estimate of the average participant. To overcome that problem, we contribute to the field with a series of experiments involving a much larger pool of participants (18–27). Our research is motivated by the lack of available data and metrics relevant for assessing the visibility of chromatic patterns in lighting applications. For example, LEDs may suffer from the color-over-angle effect, in which color varies with the angle of emitted light, leading to colored rings in projected light spots.

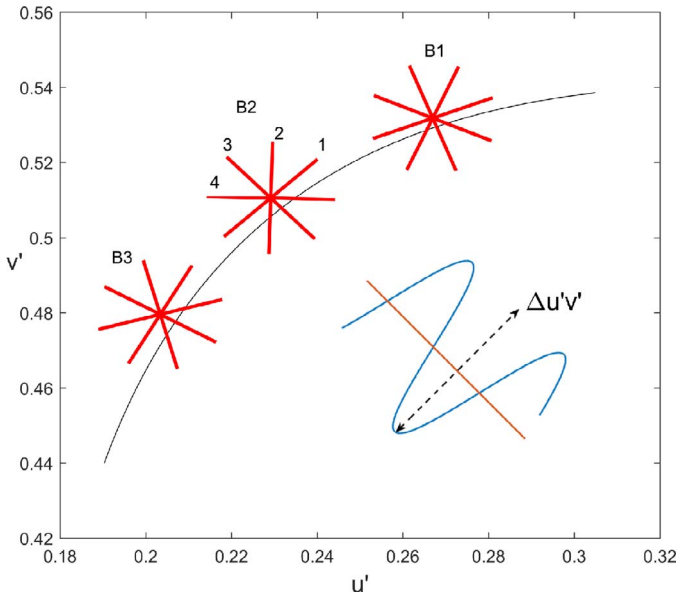

Figure 1. Black body locus (solid black line) in CIE 1976 u′v′ color space and directions of chromatic modulation at the three base colors B1, B2, B3 (approximate correlated color temperature 2600, 3800, 5700 K). Color direction 1 is parallel to the black body locus, the other directions are approximately 45° rotated counterclockwise from the previous one. Inset shows the chromatic modulation depth (top to bottom of the sinewave modulation).

Current color difference metrics are not suited for this type of application since they were derived for small-sized uniform color samples viewed side by side. We therefore set out to measure the chromatic visibility threshold in a range of spatial frequencies and base colors relevant to lighting applications. In the first part of this paper we present two experiments: Experiment 1 investigates the effect of spatial frequency, base color and direction of the chromatic modulation. Part of the results has already been published (Vogels & Lambooij, 2014), but here we show additional analyses. Experiment 2 focusses on low spatial frequencies and the number of cycles presented in the gratings. In the second part of this paper we present a modeling study that quantitatively describes the measured threshold data in terms of cone excitations and contrasts.

Methods

The goal of the two experiments was to measure the visibility threshold of chromatic sine-wave gratings as a function of several stimulus characteristics. The stimuli, experimental set-up, and procedure for the two experiments were very similar. The gratings were spatial, one dimensional sine-wave modulations of the chromaticity in particular directions in the chromaticity plane (i.e., with constant luminance) around a specific base color, which acted as the adapting color. The stimuli were generated on a calibrated color display. A staircase procedure was used to determine the chromatic contrast (or modulation depth) at which a participant correctly responded to the orientation of the grating (either horizontal or vertical) at a probability of 75%, which corresponds to a 50% detection threshold in a classical yes-no experiment (Levitt, 1971; Kaernbach, 1991).

Webster, De Valois, and Switkes (1990) have shown that systematic differences exist in the contrast thresholds

Figure 2. Examples of the stimuli (Experiment 1) at high chromatic contrast, all oriented vertically (the sine-wave direction is vertical, resulting in horizontal sinusoidal patterns). Top to bottom: base color B1, B2, B3. Left to right: color direction 1, 2, 3, 4 (see Figure 1 also). Target stimulus area subtended a visual angle of 18.9°. Examples shown here were generated at a spatial frequency of 0.5 cycles/deg and modulation depth 0.05 Δu′v′.

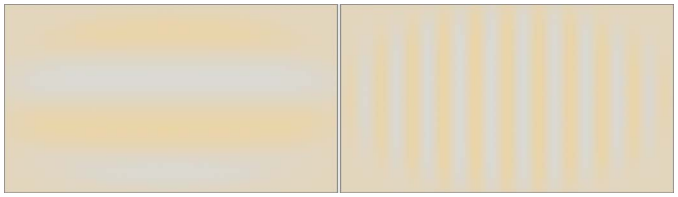

Figure 3. Examples of stimuli (in high visibility) used in Experiment 2, showing spatial frequencies of 0.05 cycles/deg in vertical grating orientation (left), and 0.15 cycles/deg in horizontal orientation (right). The stimulus area was horizontally stretched to allow the display of lower spatial frequencies (in combination with a reduced viewing distance). For a given spatial frequency, the number of cycles for the horizontal grating orientation (vertical pattern) was higher than for vertical orientation.

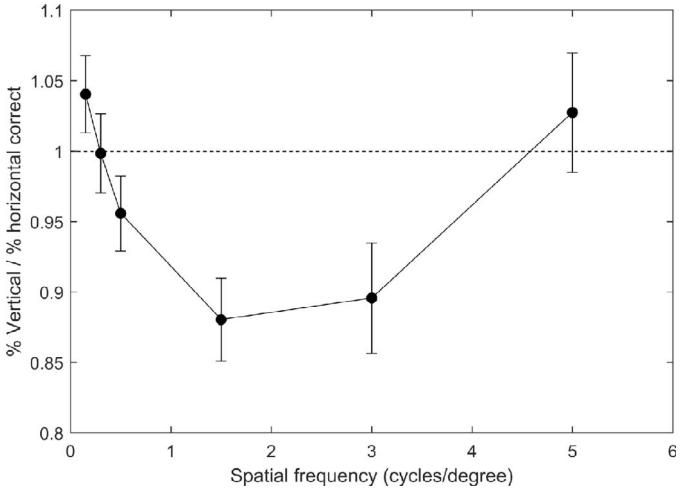

Figure 4. Vertical to horizontal ratio of the percentages correct response, averaged across all participants, base colors, directions of chromatic modulation, and levels of chromatic modulation. Error bars indicate 95% CI. Data points are connected by straight lines for clarity.

for a detection task and an orientation discrimination task. Their figure 9 plots these differences as a function of the difference in grating orientation, and shows that for a 90° orientation difference (as applies to our horizontal vs. vertical task) the contrast thresholds are identical. So, we may assume that the contrast thresholds we measure are not different from the thresholds measured by a simple detection task (detecting in which interval the grating is presented in).

Stimuli

The choice of the base color and the directions in color space of the chromatic modulations was made in the CIE 1976 u′v′ color space, which represents a perceptually uniform color space in approximation for side-by-side presentation of two colored surfaces (CIE, 2004). In Experiment 1, we selected three base colors located near the black body line, in the color temperature range 2600–5700 K, relevant for lighting applications. These base colors are indicated by B1, B2, and B3 in Figure 1, with associated (u′, v′) chromaticities of (0.2670, 0.5319), (0.2291, 0.5106) and (0.2035, 0.4796), respectively. At each base color, four color directions were defined. The first direction is parallel to the black body locus at the point of the base color, the other directions are approximately 45° rotated counterclockwise from the previous one. Along these directions, the strength of the chromatic modulation was varied in terms of $\Delta u'v'$, which was twice the Euclidian distance from the top of the modulation to the base color. The amplitude of the modulation ranged from $\Delta u'v' = 0.03$ (clearly visible) to 0 (invisible). In the range 0 to 0.01 steps of 0.0001 $\Delta u'v'$ were created, and in the range 0.01 to 0.03 steps of 0.001 $\Delta u'v'$. Examples of the sine-wave stimuli at high visibility are shown in Figure 2. Six spatial frequencies were used: 0.15, 0.30, 0.50, 1.5, 3.0, and 5.0 cycles/deg. The sine wave gratings were multiplied with a 2D attenuation profile centered on the display to smoothly blend them in the surrounding base color (matching the average stimulus color). The attenuation profile is described by

$$\text{attenuate} = 2^{-\left[2\left(X^2+Y^2\right)^{0.35}\right]^{12}} \quad (1)$$

in which X and Y represent coordinates in the range (−0.5, 0.5) relative to the display center. This attenuation profile is flat and equal to 1 at the central stimulus area and rapidly falls off to the value of 0 to the edge of the stimulus area (18.9°).

In the top part of Table 2 the number of sine-wave cycles for the experimental conditions in Experiment 1 is shown. At our lowest spatial frequency in Experiment in 1 (0.15 cycles/deg) the number of cycles was only 3, which is below the critical value of 4–5 reported for the achromatic domain (Howell & Hess, 1978; Mullen, 1985; Savoy & McCann, 1975). Below the critical value, contrast sensitivity is mainly determined by the number of cycles, and above that value by spatial frequency. Mullen (1991) showed the effect of the number of cycles for the chromatic case, but only for a single participant at 42 cd/m2. To further investigate the contrast sensitivity at low spatial frequencies, we measured the visibility thresholds at spatial frequencies of 0.025, 0.05, 0.1, 0.15, and 0.3 cycles/deg in Experiment 2. The higher spatial frequencies of 0.15 and 0.3 cycles/deg were chosen to replicate Experiment 1. In Experiment 2 the viewing distance was reduced to 0.5 m (in Experiment 1 it was 1 m). Furthermore, the target

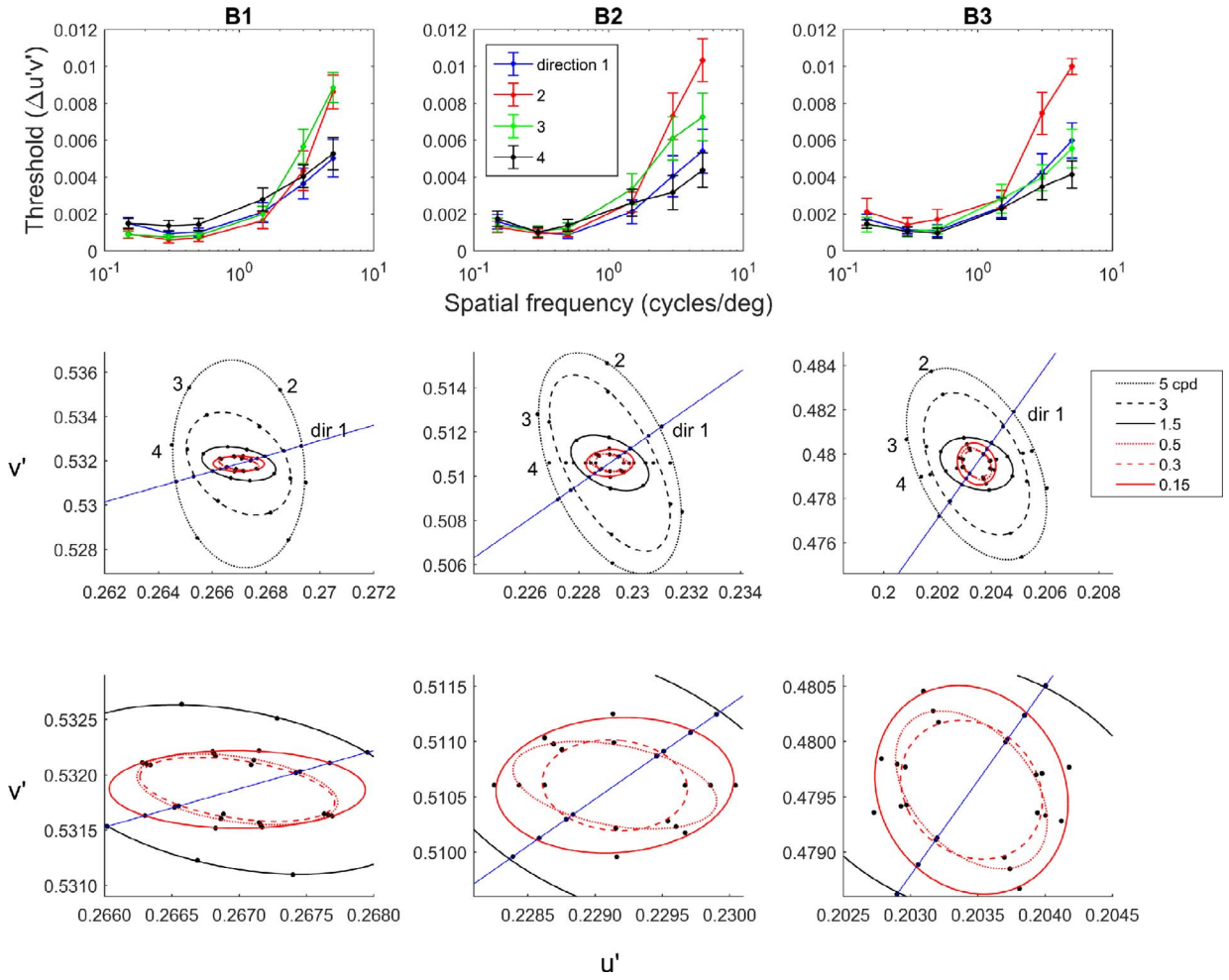

Figure 5. Results of Experiment 1. Left to right: base color B1, B2, B3. Top row shows the visibility thresholds, averaged across participants, as a function of spatial frequency. Error bars are the 95% CI of the mean. The two lower rows show the data in u′v′ color space, where for each spatial frequency an ellipse is fitted. The straight blue line indicates the first color direction (see Figure 1), which is parallel to the black body line. The other color directions are labeled counterclockwise. Note that both size and orientation of the ellipses vary with base color and spatial frequency. Bottom row is a zoom-in to better show the threshold ellipses for the lower spatial frequencies. Note that the ellipse for the lowest spatial frequency (0.15 cycles/deg) is not the smallest one.

stimulus area was extended along the horizontal direction of our display (see Figure 3 for examples). This means that although the stimulus area was fixed, for a given spatial frequency the number of cycles shown differed with grating orientation. As Table 2 shows, in Experiment 2 the number of cycles for the horizontal orientation was higher than that for the horizontal orientation. Instead of a random assignment of horizontal or vertical stimuli in a condition as in Experiment 1, orientation was now an independent variable, i.e., all conditions were shown both horizontally and vertically. The measurements in Experiments 2 were restricted to base color B2 and the first chromatic direction (i.e., tangential to the black body locus at B2, see Figure 1).

Equipment

Stimuli were presented on a 27 in. NEC Spectraview 271 display with a native spatial resolution of 2,560 × 1,440 pixels and a color resolution of 10 bits per color channel (14 bits internal processing). A PM-1423E (ProMetric; Radiant Vision Systems, Redmond, WA) imaging colorimeter was used for spatial uniformity and a PR-680L SpectraDuo spectrophotometer (Photo Research Inc, Syracuse, NY) for colorimetric characterization of the display. We used display gamma values 1.0 for all three primary channels, with which an average color precision of 0.000058 Δu′v′ across our stimulus set was calculated using a standard display characterization model (Berns, 1996).

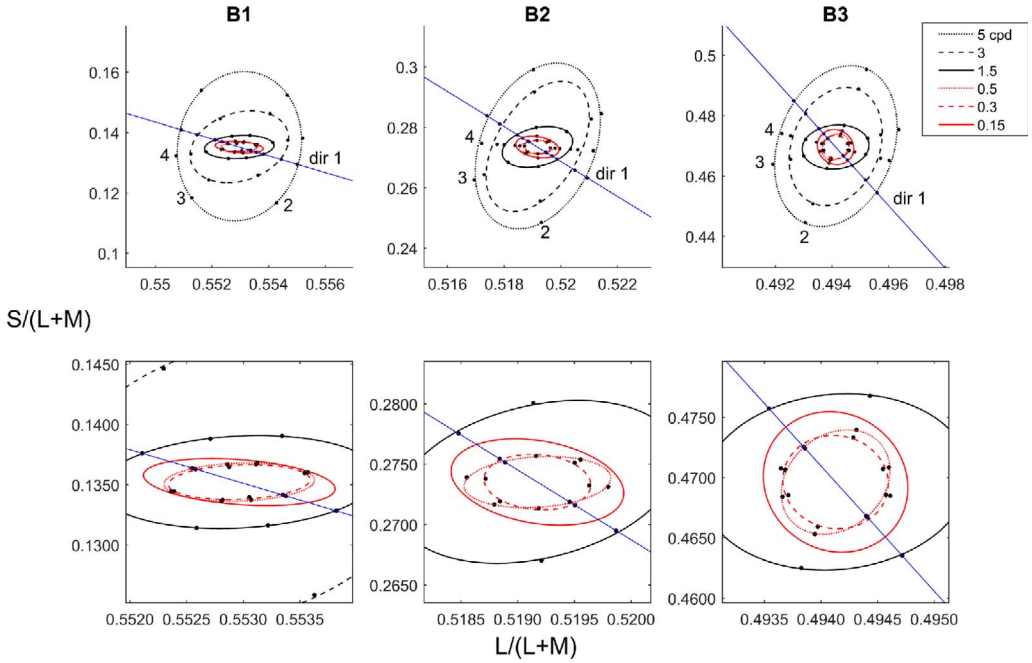

Figure 6. Results of Experiment 1, as Figure 5, now plotted in L/(L+M) versus S/(L+M) cone space. The straight blue lines indicate the first chromatic direction; the others are indicated by their number. Note the different scaling for the S/(L+M) axis.

Participants

Participants were students and employees working at Philips Research, all naïve as to the purpose of the experiment. All participants had normal color vision as confirmed with the Ishihara color vision test (24 plates edition), and normal or corrected-to-normal visual acuity as tested with a Landolt-C test chart (Laméris OoTech, Ede, The Netherlands). In Experiment 1, 18 persons participated (six female and 12 male), varying in age from 19 to 38 years. In Experiment 2, 27 persons participated (11 female and 16 male), varying in age from 19 to 51 years, with an average age of 28.6 (SD = 8.6).

Procedure

Before participants conducted the actual experiments, they read and signed an informed consent form. Then their vision was tested. If they had normal color vision and a visual acuity of 1 or better (which was the case for all our participants), they were given oral instructions on the experimental procedure. Partici-

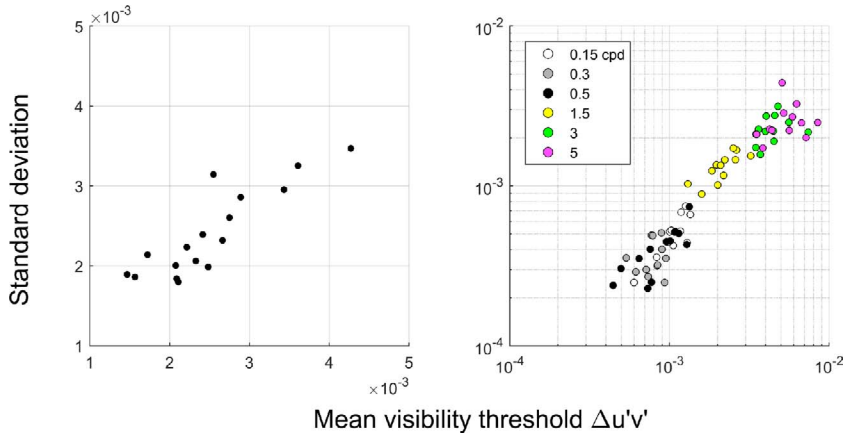

Figure 7. Standard deviation versus the mean visibility threshold. The visibility threshold ($\Delta u'v'$) is the modulation depth, that is, the difference between the top and bottom of the sine-wave chromatic modulation. Left: averaged across 72 conditions, per participant (18 data points, one per participant). Right: averaged across 18 participants, per condition (72 data points). The legend shows the different spatial frequencies. Note the log-log scale on the right-hand figure.

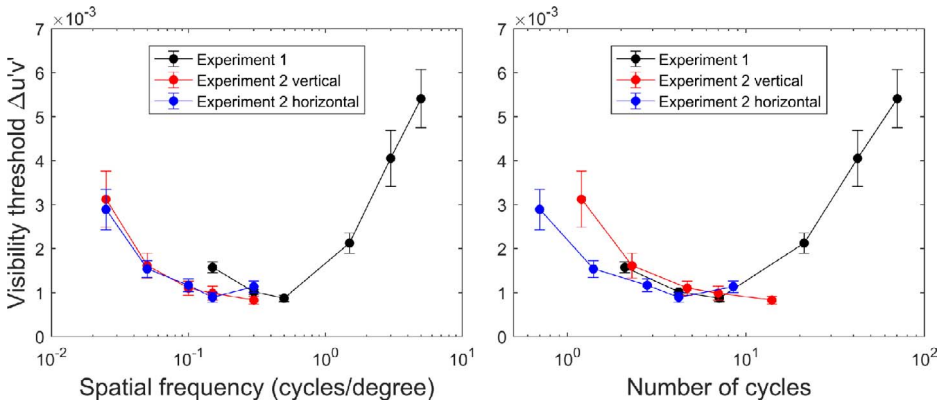

Figure 8. Mean visibility thresholds for the low spatial frequencies in Experiment 2, plotted as a function of spatial frequency (left) and effective number of cycles (right). The effective number of cycles is explained in Table 2. Data points are connected by straight lines, for convenience. Error bars indicate 95% CI. Also shown are the thresholds measured in Experiment 1, for the corresponding condition (base color B2, color direction tangential to black body locus).

pants were asked to sit on a chair in front of the display and place their head in a chinrest with forehead support, to maintain a fixed viewing distance during experimental trials. Viewing distance was 1 m in Experiment 1 and 0.5 m in Experiment 2. The participants used binocular and free-viewing, with their natural pupils. The room in which the experiments were conducted was dark except for the light coming from the stimulus display.

On the calibrated color display, participants were shown chromatic sine-wave patterns at isoluminance ($Y = 108$ cd/m^2), oriented either horizontally or vertically. In Experiment 1 the orientation was randomly assigned per trial, in Experiment 2 all stimuli were shown in both orientations. The perceived orientation of the pattern was indicated by the participants by pressing the left or right arrow key for horizontal, and up or down arrow key for vertical orientation on a keyboard. Visibility thresholds were determined using a one-down/three-up

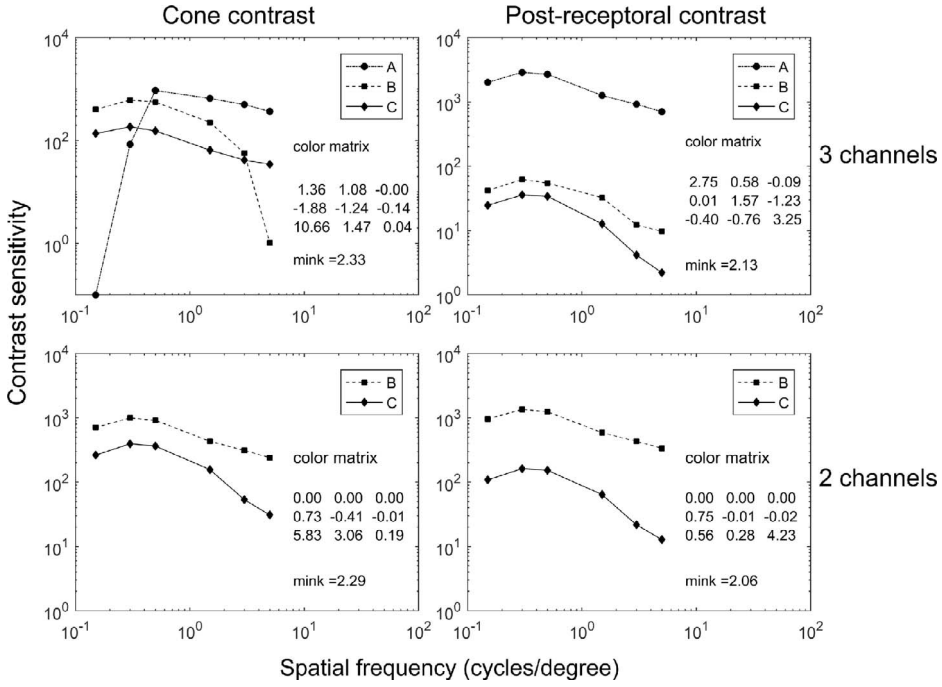

Figure 9. Model fits, showing the contrast sensitivity versus spatial frequency. Data points (markers) are connected by straight lines for clarity. Cone contrast models are on the left, postreceptoral contrast models on the right. The three-channel models are shown in the top panels, the two-channel models in the bottom panels. On the right side in each graph the estimated parameter values for the color matrix (Equation 3 or 6) and the Minkowski norm are shown. Note the different vertical scale for the top-left graph.

Experiment	Viewing distance (m)	Stimulus area	Spatial frequency (cycles/deg)	Number of cycles in stimulus area: Horizontal grating	Number of cycles in stimulus area: Vertical grating
1	1.0	Circular	0.15	2.8 (2.1)	2.8 (2.1)
		18.9°	0.30	5.7 (4.2)	5.7 (4.2)
		(14.1°)*	0.5	9.5 (7.1)	9.5 (7.1)
			1.5	28.4 (21.2)	28.4 (21.2)
			3	56.7 (42.3)	56.7 (42.3)
			5	94.5 (70.5)	94.5 (70.5)
2	0.5	Horizontally stretched ellipse	0.025	1.6 (1.2)	0.9 (0.7)
		62.8° × 37.8°	0.05	3.1 (2.3)	1.9 (1.4)
		(46.6 × 28.2°)*	0.1	6.3 (4.7)	3.8 (2.8)
			0.15	9.4 (7.0)	5.7 (4.2)
			0.3	18.8 (14.0)	11.3 (8.5)

Table 2. Number of sine-wave cycles in the target stimulus area at the different spatial frequencies. *Notes*: Effective stimulus area at 50% attenuation (and number of cycles) indicated in parentheses. * = effective stimulus area at 50% attenuation by the blending profile.

weighted staircase method that converges to 75% correct responses (Kaernbach, 1991; Levitt, 1971). There was no reason to expect a response bias in the judgment of a horizontal or vertical grating. Research has shown inconclusive results on the effect of orientation on chromatic contrast sensitivity. Kelly (1975) reported no oblique effect on the contrast sensitivity to chromatic stimuli. Murasugi and Cavanagh (1988) showed an orientation effect for a 2° red-green sinewave grating (drifting at 2 Hz). Three participants had higher sensitivity to horizontal orientation, but in the fourth participant the effect was inverted. Webster et al. (1990) showed an estimated 10% difference in contrast threshold (for both L-M grating and an S gratings) at 90° orientation difference, but only for a spatial frequency of 2 cycles/deg.

To accelerate the converging process of the staircase procedure, we applied a gain factor to the basic step size (0.0001 $\Delta u'v'$). This gain factor (initial value 10) was decreased after each second reversal point in the staircase: from 10 to 5, 2, and 1. A reversal in the staircase was obtained when a correct response was followed by an incorrect response (after which $\Delta u'v'$ was increased) or vice versa ($\Delta u'v'$ decreased). Since the starting point was always 0.03 $\Delta u'v'$ and steps 0.001 down to a $\Delta u'v'$ of 0.01, this resulted in a first series of stimuli having 0.03 $\Delta u'v'$, 0.02 $\Delta u'v'$ and 0.01 $\Delta u'v'$ modulation depth, which was implemented to clearly show the task to the participants. Below a modulation depth of 0.01 $\Delta u'v'$, steps changed to 0.0001 $\Delta u'v'$ and depending on the gain in step size, resulted in different stimulus strengths. The staircase procedure stopped after eight reversal points, and the stimulus levels at the last five reversal points were averaged to determine the visibility threshold. The staircases were interleaved at random.

After each response, a uniform adaptation image was presented for one second having the same chromaticity as the base color, but at slightly lower luminance to distinguish it from the target stimulus display. At the beginning of a session, this adaptation image was shown for 10 s to allow the participants to chromatically adapt. Full chromatic adaptation requires about 2 min (Fairchild & Reniff, 1995; Rinner & Gegenfurtner, 2000), and after 10 s the proportion of adaptation is already around 60%–70%. This was considered adequate, since the stimuli at the beginning of the session were presented at maximum chromatic modulation (i.e., highest visibility). Once the staircase procedure arrives at lower visibility levels, full adaptation had already been reached. No feedback was given on the correctness of the indicated stimulus orientation.

Experimental sessions, studying one base color at a time for adaptational reasons, lasted for about half an hour. The experiments were performed in accordance with the Declaration of Helsinki and were approved by the institutional ethics committee of Philips Research.

Experiment 1: Effect of base color, spatial frequency and chromatic direction

Experiment 1 was a full-factorial within-subject design where we measured the visibility thresholds for three base colors, four color directions and six spatial frequencies, in total $3 \times 4 \times 6 = 72$ conditions. These were divided over three sessions in which base color was kept constant to allow chromatic adaptation. The orientation of the sine-wave grating for each unique

combination of base color, chromatic direction, and spatial frequency was randomly assigned (horizontal or vertical).

Results

Orientation

In total 46,956 responses were recorded from 18 participants. In 50.05% of the trials the grating was presented in vertical orientation, and 49.95% in horizontal orientation. In the following, with a "correct response," we mean that the grating orientation as indicated by the participant was the same as the presented grating orientation. For the vertically presented gratings, 83.3% of the participant responses were correct, whereas for the horizontally presented gratings the percentage correct was 86.6%. These percentages were accumulated over all possible combinations of base color, chromatic direction, chromatic contrast, and spatial frequency. This difference in percentage correct already indicates that, on average, the horizontal gratings (vertical patterns) are slightly better detected than the vertical gratings. In Figure 4 we show a more detailed picture. For each condition (unique combination of base color, chromatic direction, spatial frequency, and chromatic contrast), we accumulated the frequencies of occurrence of the horizontal and vertical stimulus presentations, and the associated percentages of correct responses. The ratio of the vertically to horizontally obtained percentages correct response is plotted for the different spatial frequencies in Figure 4. Except for spatial frequencies 0.3 and 5 cycles/deg, the mean ratios are significantly different from 1 (p values 0.0041, 0.914, 0.0012, <0.001, <0.001, 0.20, respectively) at the 95% CI. Note that these ratios are calculated over all levels of the chromatic contrast, so including values below, around, and above threshold.

Thresholds

The top graphs in Figure 5 show the measured visibility thresholds as a function of spatial frequency for the three base colors. Data points are the thresholds averaged across participants, and the error bars are the 95% CI of the mean. For clarity, data points of the same chromatic orientation are connected with straight lines. The graphs show a minimum at the second or third spatial frequency (0.3 or 0.5 cycles/deg) and then an increasing threshold towards the higher spatial frequencies. The bottom graphs show the same data, now plotted in u′v′ color space, where ellipses were fitted with a least-squares procedure that minimizes the sum of squared orthogonal distances from the points to the fitted ellipse. This way, the points in the four color directions of equal spatial frequency are connected (each subplot shows six ellipses). There was an extremely high goodness of fit (maximum $\Delta u'v' = 10^{-6}$). The ellipses are approximately centered on the base color and, at first impression, show an increasing size with increasing spatial frequency. So, chromatic contrast sensitivity (the inverse of threshold modulation depth) is lower for the higher spatial frequencies, which is the expected result for a low-pass sensitivity function usually associated with chromatic channels. Moreover, the ellipses also rotate in u′v′ space which is not easily understood and is certainly not confined to this particular choice of color space. For instance, in Figure 6 we show the same data plotted in MacLeod-Boynton chromaticities L/(L+M) versus S/(L+M) (CIE, 2015) . The vertical axes in this figure are on a different scale than the horizontal axes, so while they may look a bit less elliptical than the plots in u′v′ space, they are actually elongated along the vertical axes when the figure is drawn on equal axis. We will show in the modeling part of this paper that the changes in size and rotation are accounted for by a chromatic detection model of the visual system.

A multiway ANOVA was performed (Matlab 2016b) to test for significant effects of the independent variables *base color*, *spatial frequency,* and *color direction* on the visibility thresholds. The threshold data were first log-transformed to obtain a normal distribution. Main effects for *base color,* $F(2, 1199) = 8.1$, $p = 0.0003$; *spatial frequency,* $F(5, 1199) = 592.18$, $p < 0.001$); and *color direction,* $F(3, 1199) = 7.56$, $p = 0.0001$, were found to be significant at the 95% CI. The first order interaction effect between *spatial frequency* and *base color* was not significant ($p = 0.0528$); the other interactions were highly significant ($p < 0.001$). One salient aspect of the thresholds shown in Figure 5 is that the ellipse size decreases with decreasing spatial frequency, but increases again for the lowest spatial frequency (0.15 cycles/deg, in bold red line). The mean threshold at spatial frequencies of 0.15 is significantly different from all others, meaning that the increase in threshold at 0.15 cycles/deg is significant with respect to the next higher spatial frequency (0.3 cycles/deg). We suspected that this was related to the diminishing number of sine-wave cycles that can be shown in a fixed stimulus area when spatial frequency is lowered. This initiated Experiment 2 in which we studied the effect of the number of cycles in the stimulus. Before presenting the results of that experiment, we first report on the variability of the thresholds between participants.

Interobserver variability

To obtain an indication of the interobserver variability, we calculated for each participant the mean visibility threshold across the 72 conditions and

the standard deviation therein. The left-hand graph in Figure 7 shows the result, where each data point represents one participant. From this figure, it is deduced that our participants differ by maximally a factor of 3 in their mean $\Delta u'v'$, and that the standard deviation in $\Delta u'v'$ increases linearly with the mean value. The latter indicates a constant coefficient of variation (standard deviation divided by the mean). The data point (participant) that stands out most is the one roughly halfway the horizontal scale and with a somewhat higher standard deviation. We could find no reason, however, to exclude the data from this participant. In the right-hand graph of Figure 7 we show a similar plot, but now the averaging is performed across participants per condition, leading to 72 data points. Spatial frequency is color coded as shown in the legend. The graph is on a log-log scale, and shows that in this case a power function would be better in place to relate the standard deviation to the mean $\Delta u'v'$. Note that both at the lowest and at the highest part of the range, the spread in the standard deviation is larger than in the middle part (corresponding to the lowest and highest spatial frequencies, respectively). Also, the mean and standard deviation in $\Delta u'v'$ threshold increase with increasing spatial frequency.

Experiment 2: Number of cycles at low spatial frequencies

For the lowest spatial frequency used in Experiment 1 we noted that the number of cycles presented in the stimulus target areas was low. In Experiment 2 we study the effect of the number of cycles in more detail, and even for lower spatial frequencies, by stretching the stimulus area and by reducing the viewing distance. Experiment 2 was a full-factorial within-subject design where we measured the visibility thresholds for one base color, one chromatic direction, five spatial frequencies and two grating orientations, in total $1 \times 1 \times 5 \times 2 = 10$ conditions. These were presented to the participants in a single session.

In Figure 8 we show the mean visibility thresholds for the low spatial frequencies used in Experiment 2, plotted as a function of spatial frequency (left plot) and as a function of the number of cycles (right plot). For comparison, also shown are the mean thresholds of Experiment 1 for the corresponding experimental condition (base color B2 and first color direction). The left figure clearly demonstrates that the increase in threshold at the lowest frequencies of the Experiment 1 data is now shifted towards lower spatial frequencies. This might be explained by the larger stimulus area in Experiment 2 (in terms of visual angle) or by the presentation of a larger number of spatial cycles. For instance, at a spatial frequency of 0.15 cycles/deg, the threshold for Experiment 2 is lower than that of Experiment 1, while both the stimulus area (18.9° circular in Experiment 1 vs. 62.8° × 37.8° elliptical in Experiment 2) and the number of cycles is larger (9.4 for horizontal and 5.7 for vertical, see Table 2). Since, an increase in stimulus area while keeping the number of cycles constant may also affect the threshold, it is difficult to conclude which of the two factors detemines the change in threshold.

As with the data of Experiment 1, a multiway ANOVA was conducted on the log-transformed threshold data of Experiment 2, using *threshold* as dependent variable and *orientation* and *spatial frequency* as independent variables. A significant main effect of *spatial frequency* on *threshold* was found, $F(4, 269) = 67.37$, $p < 0.001$. The main effect of *orientation* was not significant, $F(1, 269) = 1.58$, $p = 0.21$. No significant interaction effect between the two independent variables was found, $F(4, 269) = 1.81$, $p = 0.13$.

Discussion of Experiments 1 and 2

We have shown that the 75%-correct visibility thresholds of chromatic sine-wave gratings at isoluminance, when plotted in the 1976 u′v′ uniform color space, are well represented by ellipses. These ellipses show substantial variation in size and orientation with variation in base color, and in particular with spatial frequency. This is fundamentally different from the well-known MacAdam ellipses (MacAdam, 1942), which are at the basis of uniform color spaces and industrial color tolerancing procedures. The MacAdam ellipses do also show a variation in size and orientation per color point when plotted in 1931 CIE *xy* color space, but the 1976 u′v′ color space was designed to minimize these variations. We here show strong additional changes in ellipse shape when spatial frequency at a fixed color point is varied within a constant stimulus size, underlining the limited applicability of the MacAdam ellipses to nonuniform stimuli. We should note that the MacAdam ellipses were measured for adaptation to the chromaticity of illuminant C, whereas in our experiments participants were adapted to base colors of correlated color temperature 2600, 3800, and 5700 K. A difference in adaptation point leads to different discrimination ellipses, as shown for example, by Opstelten and Rinzema (1987) and by Krauskopf and Gegenfurtner (1992). Moreover, MacAdam used a 2° bipartite test field having a luminance of about 48 cd/m^2, twice that of the background, whereas we used

isoluminant sine-wave patterns at 108 cd/m^2. So, the two types of stimuli also have very different spatial frequency content.

On the lower end of the spatial frequency scale, we find an effect of the number of cycles. This confirms the work of Mullen (1991) who measured the change in contrast sensitivity for different number of cycles, but only for a red-green grating at 42 cd/m^2 and for a single participant. Also in the achromatic domain it has been reported that the number of cycles becomes dominant in contrast sensitivity measurements at the lowest spatial frequencies (Savoy & McCann, 1975). This is linked to the fact that the physical limitations in display size simply do not allow the presentation of more cycles. Decreased sensitivity in that case is not necessarily caused by the visual system, but may result from a methodological artefact. Rovamo et al. (1993) described contrast sensitivity in the luminance domain as a function of stimulus size, spatial frequency, and number of cycles. In the chromatic domain, however, the effects of the interplay of these parameters have not been unified into a single model yet.

With respect to the orientation of the sine-wave gratings, for spatial frequencies in the range 0.5–3 cycles/deg used in Experiment 1 we find that the average sensitivity to horizontally oriented gratings is slightly higher than for vertical gratings. This is also visible in Figure 8, where the right-hand graph shows that at a given number of spatial cycles (less than 10), the threshold for horizontal is lower than for vertical grating orientation. Interestingly, the mean threshold-ratio reported by Webster et al. (1990) for 90° orientation difference, measured at 2 cycles/deg, differed about 10% from the value of 1, which corresponds well with our data measured at 1.5 and 3.0 cycles/deg (see Figure 3).

Modeling the chromatic visibility threshold

In this section, we present a model of the participant-averaged threshold data of Experiment 1. We do not include the threshold data from Experiment 2 since it involves different spatial parameters (elliptical vs. circular stimulus area, different visual angles). Another reason for omitting the data of Experiment 2 is the difference in retinal illumination level, caused by the difference in viewing distance for the two experiments (1 m in Experiment 1 and 0.5 m in Experiment 2). At half the viewing distance, corneal illuminance increases by a factor of about 4, assuming the inverse square law to apply here. Although we did not measure actual pupil sizes, we estimated these by applying the formula for the light-adapted pupil size by Watson and Yellott (2012) to our experimental conditions, which includes angular stimulus size and luminance. For a 30-year-old, pupil sizes of 3.42 and 2.94 mm were calculated for Experiment 1 and 2. So indeed, different retinal illuminance levels were involved in the two experiments.

As a first step, we need to convert the threshold data from u′v′ space to cone excitation space. Cone excitations are obtained by multiplying the spectral power distributions emitted by the display with the cone fundamentals (CIE, 2006). For convenience, to allow easier calculations and transformations in u′v′, XYZ and LMS space, for our NEC display we also derived the following matrix relationship between CIE 1931 XYZ tristimulus values and LMS cone excitations:

$$\begin{pmatrix} L \\ M \\ S \end{pmatrix} = \begin{pmatrix} 0.34687 & 1.07301 & -0.04871 \\ -0.59010 & 1.80232 & 0.15324 \\ 0.02061 & -0.04607 & 1.32477 \end{pmatrix} \begin{pmatrix} X \\ Y \\ Z \end{pmatrix}. \quad (2)$$

Conversion from u′v′ space to cone excitation space is then achieved by first converting u′v′Y to XYZ, and then applying Equation 2 to obtain the L, M, and S cone excitations.The matrix elements in Equation 2 were calculated by minimizing the pooled model error for a set of 27 spectral measurements, where for example, L is modeled as $L = m_{11} \times X + m_{12} \times Y + m_{13} \times Z$ and m_{1j} represent the matrix elements in the first row. The average absolute error was 0.0001, negligibly small compared to the cone excitation values of around 100.

The next step is to transform the cone excitations from the base color and those from the threshold values into chromatic mechanisms, by linear recombination. We here study two such transformations, differing in the stage at which a contrast signal is calculated. In the first transformation, which we refer to as the "cone contrast" model, cone-specific contrasts are calculated before they are converted into chromatic mechanisms. This type of transformation is for instance reported by Brainard (1996) and Wuerger et al. (2002). In the second transformation, which we will refer to as the "postreceptoral contrast" model, contrast signals are calculated within the chromatic mechanisms, after these are constructed from linear recombination of the L, M, and S cone excitations. In addition, for both models we study the impact of having two or three chromatic mechanisms on the explained data variance. We expect a model with two chromatic channels to be more appropriate for our experimental data, since it represents chromatic

thresholds at isoluminance, that is, one of the color dimensions is silenced.

Cone contrast model

In the cone contrast model, a contrast signal is computed at the cone receptor level as $\Delta L/L$, $\Delta M/M$, $\Delta S/S$, where $\Delta L/L$ for instance is calculated as $(L_{\text{threshold}} - L_{\text{base color}})/ L_{\text{base color}}$, that is, the threshold increment or decrement relative to the level of the base color, which is assumed to correspond to the adapting color. Using a 3×3 matrix, we linearly recombine these cone contrasts into chromatic channels, here arbitrarily labeled as A, B, C:

$$\begin{pmatrix} A \\ B \\ C \end{pmatrix} = \begin{pmatrix} a_{11} & a_{12} & a_{13} \\ a_{21} & a_{22} & a_{23} \\ a_{31} & a_{32} & a_{33} \end{pmatrix} \begin{pmatrix} \Delta L/L \\ \Delta M/M \\ \Delta S/S \end{pmatrix}. \quad (3)$$

Next, the values in the A, B, and C channels are weighted by sensitivity functions S_i (i = A, B, C) that depend on spatial frequency f, and we then apply probability summation with a Minkowski norm to compute a pooled detection signal:

$$\text{signal}_{cc} = [|A\ S_A(f)|^p + |B\ S_B(f)|^p + |C\ S_C(f)|^p]^{\frac{1}{p}} \quad (4)$$

where subscript cc stands for cone-contrast and p represents the Minkowski norm coefficient. In the data fitting procedure (least squares) we simultaneously optimize the matrix elements in Equation 3, the sensitivities $S_A(f)$, $S_B(f)$, $S_C(f)$ at each spatial frequency, and the Minkowski coefficient in Equation 4 to minimize the pooled model error:

$$\text{error}_{cc} = \sum_{i=1}^{72} [1 - \text{signal}_{cc}(i)]^2 \quad (5)$$

where the summation runs over the 72 experimental conditions (3 base colors $\times$ 4 chromatic directions $\times$ 6 spatial frequencies). For a model perfectly fitting the experimental data the pooled error would be zero and all values for $\text{signal}_{cc}(i)$ would equal 1, which is an arbitrary choice but conveniently indicates the threshold level. In the case of the three-channel model we have 28 parameters to estimate (i.e., 9 matrix coefficients in Equation 3 for the color transformation, $3 \times 6 = 18$ for the spatial sensitivity, and the Minkowski coefficient). In the case of the two-channel model, we arbitrarily omit channel A and matrix coefficients a_{11}, a_{12}, a_{13} in Equation 3, and we also leave out the corresponding contrast signal A in Equation 4. Optimization of the two-channel model thus requires the estimation of 19 parameters (i.e., 6 color matrix coefficients + 2×6 spatial sensitivities +1 Minkoswki coefficient).

Postreceptoral contrast model

In the postreceptoral contrast model, we first use a 3×3 matrix to linearly recombine L, M, and S cone excitations into chromatic channels

$$\begin{pmatrix} A \\ B \\ C \end{pmatrix} = \begin{pmatrix} b_{11} & b_{12} & b_{13} \\ b_{21} & b_{22} & b_{23} \\ b_{31} & b_{32} & b_{33} \end{pmatrix} \begin{pmatrix} L \\ M \\ S \end{pmatrix}. \quad (6)$$

Contrast signals within these chromatic channels are then calculated as $\Delta A/A$, $\Delta B/B$ and $\Delta C/C$, where $\Delta A/A$ for instance is calculated as $(A_{\text{threshold}} - A_{\text{base color}})/ A_{\text{base color}}$, that is, the threshold increment or decrement relative to the level of the base color. The contrast signals are weighted by a sensitivity function S that depends on spatial frequency (f), and we then apply probability summation with a Minkowski norm to compute a detection signal:

$$\text{signal}_{prc} = \left[\left|\frac{\Delta A}{A} S_A(f)\right|^p + \left|\frac{\Delta B}{B} S_B(f)\right|^p + \left|\frac{\Delta C}{C} S_C(f)\right|^p\right]^{\frac{1}{p}} \quad (7)$$

where subscript prc stands for postreceptoral contrast. As for the cone contrast model, we estimate 28 parameters for the three-channel model and 19 parameters for the two-channel model, by minimizing the pooled error

$$\text{error}_{prc} = \sum_{i=1}^{72} \left[1 - \text{signal}_{prc}(i)\right]^2. \quad (8)$$

Model selection

In Figure 9 the estimated parameter values for the four different models are shown. The plotted lines connect the estimated contrast sensitivities of the chromatic channels (S_A, S_B, and S_C) at the six spatial frequencies, next to these the values of the nine coefficients in the color matrix and the Minkowski norm parameter are shown. In general, the sensitivity functions show a low-pass behavior for spatial frequency, except for the data point at the lowest spatial frequency (0.15 cycles/deg). Also, the sensitivity curve for channel B in the three-channel cone contrast model (top left graph) is more of a band-pass type typically found for an achromatic channel. Indeed, the coefficients in the corresponding color matrix show that the channel is constructed by mainly adding L and M cone excitations (the achromatic channel is usually defined as L+M).

The difference in magnitudes of the contrast sensitivities is linked to the difference in magnitudes of the contrast signals. The product of contrast and sensitivity is balanced for the channels. For example, in the two-

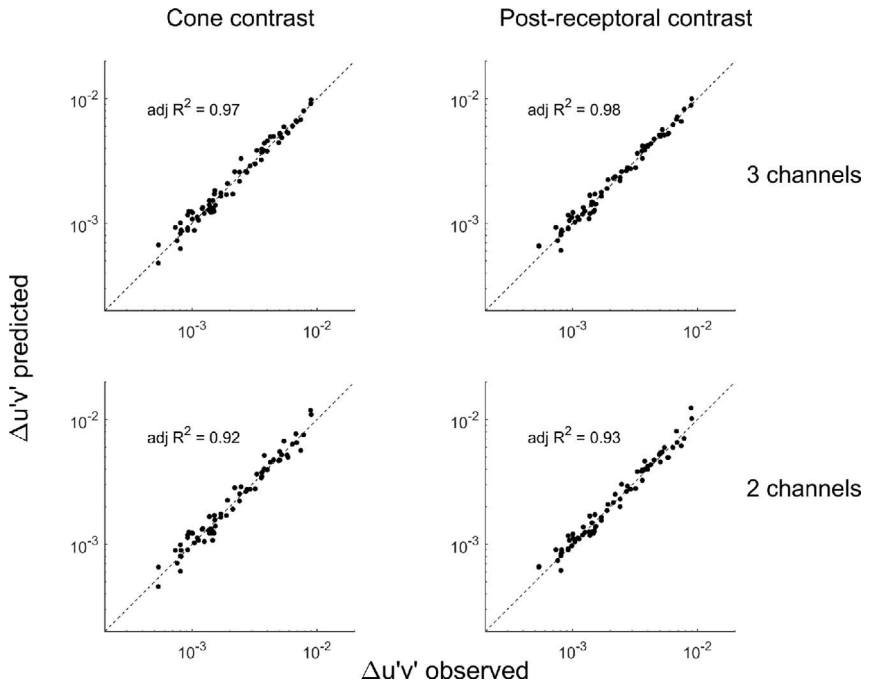

Figure 10. Predicted versus observed $\Delta u'v'$ thresholds, for all 72 conditions. Predictions were made with the cone contrast model (left) and the postreceptoral contrast model (right), either with three chromatic channels (top) or two (bottom). Perfect correlation would be indicated by all data points falling on the dashed identity line. Also shown are the adjusted R^2 values of the fits (i.e., R^2 corrected for the number of fitted parameters).

channel postreceptoral contrast model (bottom right graph) the sensitivity of the B-channel is about 10 times as high as that of the C-channel. This factor of 10 is reflected in the mean absolute values of the contrast signals $\Delta B/B$ and $\Delta C/C$, which are 0.0011 and 0.014, respectively.

The optimized Minkowski rank parameter is around 2.1 for the postreceptoral contrast models and around 2.3 for the cone contrast models, in both cases not very different from 2. The latter would indicate that the threshold response of the visual system to a sine-wave chromatic stimulus of a single spatial frequency is approximated by a common Euclidean distance metric.

In Figure 10 we show the predicted versus observed chromatic visibility thresholds for the four models (note the logarithmic scale). The plotted $\Delta u'v'$ value is the chromatic modulation depth as shown in Figure 1, the Euclidian distance in $u'v'$ color space between the top and the bottom of the chromatic modulation. All color directions, base colors, and spatial frequencies are plotted here, resulting in 72 data points. A perfect model would have all data points coinciding with the dashed identity lines. Visually judging from Figure 10, all models show excellent fits to the data, implying that they successfully account for the size and orientation of the threshold ellipses shown in Figure 5. The question arises, however, which is the best performing model. Based on the values of the adjusted R^2 only (shown in Figure 10), it would be concluded that the three-channel models outperform the two-channel models. However, the contrast signals in two channels of the three-channel models were highly correlated, indicating an overfit, whereas the contrast signals in the two-channel models were almost uncorrelated. In the next section we use the Akaike Information Criterion to compare the models and show that a model having two chromatic channels is more likely than one having three, and postreceptoral contrast calculation is much more likely than cone contrast.

Akaike Information Criterion

To compare the performance of the different models in more detail, we here use Akaike's Information Criterion, abbreviated as AIC, (Akaike, 1974; Burnham & Anderson, 2002). This criterion is often used to judge how well observed data is fitted by a model while considering the number of free model parameters. The underlying idea is that when allowing a higher model complexity, that is, a higher number of free parameters, a penalty is raised for the lack of parsimony.

In the case of least squares regression, assuming normally distributed model errors with constant variance, the AIC value is calculated with the following equation (Burnham & Anderson, 2002):

$$\mathrm{AIC}_c = n \ln\left(\frac{\mathrm{RSS}}{n}\right) + 2K + \frac{2K(K+1)}{(n-K-1)} \quad (9)$$

Model	Contrast model	Chromatic channels	Fitted parameters	RSS	AIC_c	Akaike weights	Evidence ratio of model 3 to model i
1	Cone	2	19	1.059	−243.3	5.57E-05	17910
2		3	28	0.671	−231.3	1.37E-07	7263894
3	Postreceptor	2	19	0.807	−262.9	9.97E-01	1
4		3	28	0.509	−251.2	2.86E-03	349

Table 3. AIC performance measures of the model fits. *Notes:* RSS is the residual sum of squares (Equation 5 and Equation 8); AIC_c is the AIC value calculated according to Equation 9.

where RSS is the residual sum of squares (the residual is the model error in Equation 5 and Equation 8), n the number of observations (72 in our case) and K the number of free model parameters, including counts for the intercept and variance of the model error. Subscript c denotes the AIC formula with sample size correction, which is advised when $n/K < 40$ (Burnham & Anderson, 2002).

Generally, the model having the lowest AIC_c value is the preferred model in the sense that it has the lowest loss of Kullback-Leibler information when approximating a true distribution with the model distribution of data values (Burnham, Anderson, & Huyvaert, 2011). From Equation 9 it follows indeed that a model having a smaller residual sum of squares gives rise to a smaller AIC_c value. In Table 3 the AIC performance measures of the model fits described above are presented. It shows two important things. Firstly, the two-channel models have lower AIC_c values (in the order of $\Delta AIC_c = 10$) than the three-channel models. Secondly, the postreceptoral contrast models have lower AIC_c values (in the order of $\Delta AIC_c = 20$) than the cone contrast models.

To determine which model is most likely to be "true", we calculated the evidence ratios of the models, as explained below. From the raw AIC_c values we calculated the so called Akaike weights (e.g., Wagenmakers & Farrell, 2004) defined as

$$w_i = \frac{\exp(-0.5\Delta_i \mathrm{AIC})}{\sum_{m=1}^{M} \exp(-0.5\Delta_m \mathrm{AIC})} \quad (10)$$

The Akaike weights are shown in the second last column of Table 3. The nominator in Equation 10 represents the relative likelihood of model i and the denominator is the sum of the relative likelihoods of all M models. The ΔAIC values appearing in Equation 10 are obtained by subtracting the minimum AIC value of the pool of models from that of model i: $\Delta_i \mathrm{AIC} = \mathrm{AIC}_{c,i} - \mathrm{AIC}_{c,min}$. The ratio of the Akaike weights of two models can be interpreted as the evidence ratio of one model to the other. The last column in Table 3 presents the evidence ratios for model three. So, the ratio of models three and four, having the lowest and second lowest absolute AIC_c value, equals $0.997/0.00286 = 349$, implying that model 3 (postreceptoral, two chromatic channels) is 349 times more likely to be the true model in comparison to the postreceptoral three-channel model. Likewise, the ratio of the Akaike weights of models three and one is $0.997/5.547\mathrm{E}-05 = 17{,}910$, indicating that within the two-channel models, the postreceptoral contrast model is much more likely than the cone-contrast model. We will come back to this salient result in the discussion section.

Discussion

Cone contrast versus postreceptoral contrast

According to Akaike's Information Criterion, a postreceptoral contrast model is much more likely than a cone-contrast model, a finding that is of interest for vision science. Another related criterion often used for model selection is the Bayesian Information Criterion or BIC (e.g., Raftery, 1995). The difference between the AIC and BIC is that the latter puts a stronger penalty on the number of free model parameters. We calculated the difference in BIC value between the postreceptoral and contrast models and arrived at a ΔBIC of around 20. The interpretation of this number (Raftery, 1995) to our set of models is that there is very strong evidence in favor of the postreceptoral contrast model. So, analysis with both AIC and BIC suggests that the computation of spatial contrast in the early stage of visual processing is most likely carried out within postreceptoral channels. This is in line with the work of Jameson and Hurvich (1955), Koenderink, van de Grind, and Bouman (1972), and the line element approach of Vos and Walraven (1972). Vos and Walraven (1972) also first decode the cone outputs into a second stage with opposed chromatic channels, before transmitting a difference signal to the brain. However, they scale the difference signals in these channels by their uncertainties, whereas in our approach the scaling is done by the signal of the base color to create a contrast signal. Guth's (1995) color vision model also incorporates an initial remapping of (compressed) cone signals into opponent channels (known as ATD). Chromatic discrimination in Guth's model can be calculated based on the Euclidian distance between two ATD vectors. It is unclear, however, how to calculate the signals for chromatic adaptation in the case of a sinusoidally varying target as we have used in our experiments.

Two versus three channels

The finding that a signal detection model with two channels is more likely than a model with three channels for describing our threshold data is also of interest. One could argue that this was expected because in our target stimuli we kept luminance constant. However, since luminance is defined by the CIE standard observer (characterizing the mean luminous sensitivity of a group of observers), for an individual observer, isoluminance may not have been guaranteed. That would have first required the measurement of an individual's sensitivities, as can be done with flicker photometry (Kelly, 1983; Luria & Neri, 1986). This was not in scope of the present study, however, since we are interested in the average observer response when using the luminance definition of the CIE standard observer. Still, for an individual observer the chromatic signals may have carried a small luminance component. Given the band-pass nature of the achromatic contrast sensitivity function at our luminance level (108 cd/m^2) and its peak around a spatial frequency of about 3 cycles/deg (Kim et al., 2013), the influence of the achromatic component would have occurred for our stimuli at 3 and 5 cycles/deg. For the lower spatial frequencies we studied, achromatic contrast sensitivity is negligibly small relative to chromatic contrast sensitivity.

Interpreting the color matrix

We return to results shown in Figure 9, where the estimated values of the color matrix are shown on the right-hand side in each graph. The values in the color matrix reveal how the L, M, and S color signals are recombined into postreceptoral channels (Equations 3 and 6). For the two-channel models, the B-channel is created mainly from L whereas the C-channel is obtained by summation of L, M, and S. These transforms do not resemble the traditional chromatically opponent channels like L-M ("red-green") and (L+M) − S ("yellow-blue"). For our best performing model, the two-channel postreceptoral contrast model, we have $B = 0.75 \times L - 0.01 \times M - 0.02 \times S$ and $C = 0.56 \times L + 0.28 \times M + 4.23 \times S$. Since the signals in B and C are further processed as contrasts, we could also rewrite them as $B = L - 0.013 \times M - 0.027 \times S$ and $C = 0.13 \times L + 0.066 \times M + S$ where we normalize on the maximum value. This shows that channels B and C are largely dominated by L and S-cone signals, respectively. This is in line with Figure 6, in which we plotted the data in terms of L/(L+M) and S/(L+M), that is, the luminance-normalized L and S cone signals. Apparently, L and S cones contribute most (but not all) to the detection of our isoluminant stimuli. This is understandable from the point of view that the L and M cone signals are highly correlated at isoluminance, whereas S cone signals are free to vary without affecting luminance. Any increase in L is associated with a decrease in M, and vice versa, since luminance is the sum of L and M. So, an information-efficient chromatic detection mechanism at isoluminance, striving for minimum redundancy, would not need signals from both L and M cones.

For the two-channel cone-contrast model, we calculated model performance when the color matrix is constrained as in part of the Wuerger et al. (2002) study. We required the sum of the row elements in the color matrix to be zero, to force chromatic opponency. The resulting channels were $B = 0.538 \times L - 0.534 \times M - 0.004 \times S$ and $C = -0.119 \times L - 0.136 \times M + 0.255 \times S$, with a Minkowski coefficient of 2.14 and a residual sum of squares (RSS) of 1.749. The latter is substantially worse than the value 1.059 reported in Table 3. Even though we had to estimate fewer parameters (because of the constraint on the color matrix) this resulted in an AIC_c value of −215, much worse than the values reported in Table 3. So, when forcing the traditional chromatically opponent channels, model performance drops substantially. In general, since our best result was obtained by estimating all model parameters in a single run, any constraint put on the model parameters will lead to a decrease in the reported performance.

We also estimated the color matrix for the case where we allow the L, M, and S cone signals to first undergo a power-transformation. So, instead of recombining linear cone signals, we let the color matrix recombine nonlinear cone signals (L, M, and S raised to the power of n_L, n_M, and n_S, respectively). For the two-channel postreceptoral model this resulted in a slightly lower RSS of 0.785 (compared to the 0.807 reported in Table 3), but at the cost of three additional model parameters. The accompanying AIC_c value was −251.9, not better than our best result.

Quantitative comparison

We simultaneously estimated the parameters in the color tuning matrix and spatial sensitivity functions, and since we have a single color matrix for all spatial frequencies, our model is of the type where space and color are separable (Poirson & Wandell, 1993). The best quantitative comparison we can make is with the study of Wuerger et al. (2002). We compare our mean squared error values with those reported in their table 4. Their best color separable model has a mean squared error of 0.138 (84 data points, 19 free parameters) when fitted over the three observers simultaneously. In comparison, for our cone-receptoral contrast model with two chromatic channels we find a mean squared error of 0.0147 (72 data points and 19 parameters), and for the postreceptoral contrast model it is 0.0112.

Although these values are both a factor of 10 lower, a direct comparison is problematic since our 72 data points were obtained by first averaging across participants. If we estimate the model parameters on the data of all 18 participants, we arrive at a mean squared error of 0.193 with $72 \times 18 = 1{,}296$ data points. We should note that in the Wuerger et al. (2002) study the chromatic contrast sensitivity functions were parameterized and constrained to be of a Gaussian shape, which may affect model residuals. In addition, their dataset included achromatic as well as mixtures of achromatic and chromatic stimuli, which limits the comparison with our chromatic-only data.

Summary and conclusions

In two experiments we systematically varied the base color, spatial frequency, and chromatic direction of isoluminant sine-wave gratings and measured their visibility thresholds for a pool of participants much larger than usually reported. Also grating orientation and the number of cycles was varied. When plotted in u′v′ color space or in cone space, our threshold data is represented by ellipses centered on the base color, whose size and orientation depends on base color and spatial frequency. Chromatic contrast sensitivity seems to drop at the lowest spatial frequency, but we showed that this is most probably due to the limited (low) number of sine-wave cycles that can be shown on the stimulus display. Our data set allowed us to test different models of chromatic contrast sensitivity in a range of base colors and spatial frequencies relevant to lighting applications. Analysis of our modeling study reveals the highest evidence for a chromatic detection model of the visual system in which the neural computation of chromatic contrast is performed within two postreceptoral channels, and not at the cone level (cone-contrast) as predominates in literature. These two channels are largely (but not fully) determined by L-cone and S-cone signals, respectively. We can understand this result by assuming that for the detection of chromatic signals in isoluminance (for which $L + M$ is constant), the visual system strives for a minimum redundancy in information processing.

Future perspective

The models described in this paper allow for the prediction of chromatic visibility thresholds for other points in color space with higher color saturation, further away from the black body locus. Experiments to gather data at base colors with higher color saturation are currently ongoing and will allow us to further evaluate and develop our models. Another interesting line of research is to study the interplay of the stimulus parameters (area, spatial frequency, number of cycles) more systematically. For instance, by changing the number of cycles at a fixed spatial frequency, the stimulus size changes also. In addition, it would be interesting to study the effect of the cycle number, as Mullen (1991) did. Finally, we believe that a color vision model that takes spatial frequency content of stimuli into account can play an important role in the development of color difference formulae and uniform color spaces.

Keywords: chromatic contrast sensitivity, visibility threshold, probability summation, model comparison, postreceptoral contrast

Acknowledgments

The authors are thankful to Tijmen Daatselaar and Jeroen Veelenturf for their assistance in Experiment 2.

Commercial relationships: Marcel Lucassen, Marc Lambooij, and Dragan Sekulovski are employees of Philips Lighting Research. Ingrid Vogels was an employee of Philips Research at the time Experiment 1 was performed, and is now with the Eindhoven University of Technology.
Corresponding author: Marcel Lucassen.
Email: marcel.lucassen@philips.com.
Address: Philips Lighting Research, High Tech Campus 7, Eindhoven, The Netherlands.

References

Akaike, H. (1974). A new look at the statistical model identification. *IEEE Transactions on Automatic Control*, *19*, 716–723.

Barten, P. G. J. (1999). *Contrast sensitivity of the human eye and its effects on image quality*. Eindhoven, The Netherlands: Technische Universiteit Eindhoven, https://doi.org/10.6100/IR523072.

Berns, R. S. (1996). Methods for characterizing CRT displays. *Displays*, *16*, 173–182.

Brainard, D. H. (1996). Cone contrast and opponent modulation color spaces. In P. K. Kaiser & R. M. Boynton (Eds.), *Human color vision* (2nd ed., pp. 563–579). Washington, DC: Optical Society of America.

Burnham, K. P., & Anderson, D. R. (2002). *Model selection and multimodel inference: A practical*

information-theoretic approach. New York, NY: Springer-Verlag.

Burnham, K. P., Anderson, D. R., & Huyvaert, K. P. (2011). AIC model selection and multimodel inference in behavioral ecology: Some background, observations, and comparisons. *Behavioral Ecology and Sociobiology*, *65*(1), 23–35.

Campbell, F. W., & Robson, J. G. (1968). Application of Fourier analysis to the visibility of gratings. *The Journal of Physiology*, *197*, 551–566.

Carlson, C. R. (1982). Sine-wave threshold contrast-sensitivity function: Dependence on display size. *RCA Review*, *43*, 675–683.

CIE. (2004). *Colorimetry* (3rd ed., Report No. 15-2004). Vienna, Austria: CIE Central Bureau.

CIE. (2006). *Fundamental chromaticity diagram with physiological axes, Part 1* (Report No. 170-1-2006). Vienna, Austria: CIE.

CIE. (2015). *Fundamental chromaticity diagram with physiological axes, Part 2: Spectral luminous efficiency functions and chromaticity diagrams* (Report No. 170-2-2015). Vienna, Austria: CIE.

Fairchild, M. D., & Reniff, L. (1995). Time course of chromatic adaptation for color-appearance judgements. *Journal of the Optical Society of America A*, *12*, 824–833.

Granger, E. M., & Heurtley, J. C. (1973). Visual chromaticity-modulation transfer function. *Journal of the Optical Society of America*, *63*, 1173–1174.

Guth, S.L. (1995). Further applications of the ATD model for color vision. *Proceedings of the SPIE 2414, Device-Independent Color Imaging II, 2414*, 12–26, https://doi.org/10.1117/12.206546.

Howell, E. R., & Hess, R. F. (1978). The functional area for summation to threshold for sinusoidal gratings. *Vision Research*, *18*, 369–374.

Jameson, D., & Hurvich, L. M. (1955). Some quantitative aspects of an opponent colors theory. I. Chromatic responses and spectral saturation. *Journal of the Optical Society of America*, *45*, 546–552.

Kaernbach, C. (1991). Simple adaptive testing with the weighted up-down method, *Perception & Psychophysics*, *49*, 227–229.

Kelly, D. H. (1975). No oblique effect in the chromatic pathways. *Journal of the Optical Society of America*, *65*, 1512–1514.

Kelly, D. H. (1983). Spatiotemporal variation of chromatic and achromatic contrast thresholds. *Journal of the Optical Society of America*, *73*, 742–750.

Kim, K. J., Mantiuk, R., & Lee, K.H. (2013). Measurements of achromatic and chromatic contrast sensitivity functions for an extended range of adaptation luminance. In B. E. Rogowitz, T. N. Pappas, & H. de Ridder (Eds.), *Proceedings of the SPIE 8651, Human Vision and Electronic Imaging XVIII*, 86511A (14 March 2013), https://doi.org/10.1117/12.2002178.

Koenderink, J. J., van de Grind, W. A., & Bouman, M. A. (1972). Opponent color coding: A mechanistic model and a new metric for color space. *Kybernetik*, *10*, 78–98.

Krauskopf, J., & Gegenfurtner, K. (1992). Color discrimination and adaptation. Vision Research, *32*(11), 2165–2175.

Levitt, H. Transformed up–down methods in psychoacoustics (1971). *Journal of the Acoustical Society of America*, *49*, 467–477.

Luria, S. M., & Neri, D. F. (1986). Individual differences in luminous efficiency measured by flicker photometry. *Color Research and Application*, *11*, 72–75.

MacAdam, D. L. (1942). Visual sensitivities to color differences in daylight. *Journal of the Optical Society of America*, *32*, 247–274.

Mullen, K. T. (1985). The contrast sensitivity of human colour vision to red-green and blue-yellow chromatic gratings. *The Journal of Physiology*, *359*(1), 381–400.

Mullen, K. T. (1991). Colour vision as a post-receptoral specialization of the central visual field. *Vision Research*, *31*, 119–30.

Murasugi, C. M., & Cavanagh, P. (1988). Anisotropy in the chromatic channel: Horizontal-vertical effect. *Spatial Vision*, *3*, 281–291.

Opstelten, J. J., & Rinzema, G. (1987). New insights in chromaticity and tolerance areas of fluorescent lamps. *Journal of the Illuminating Engineering Society*, *16*(1), 117–127.

Owens, H. C., Westland, S., Van de Velde, K., Delabastita, P., & Jung, J. (2002). Contrast sensitivity for lime-purple and cyan-orange gratings. In *IS&T/SID Tech Color Imaging Conference* (pp. 145–148).

Poirson, A. B., & Wandell, B. A. (1993). Appearance of colored patterns: Pattern-color separability, *Journal of the Optical Society of America A*, *10*, 2458–2470.

Raftery, A. E. (1995). Bayesian model selection in social research. In P. V. Marden (Ed.), *Sociological methodology*, (pp. 111–163). Cambridge, MA: Blackwells.

Rajala, S. A., Trussell, H. J., & Krishnakumar, B.

(1992). Visual sensitivity to color-varying stimuli. *Proceedings of the SPIE*, *1666*, 375–386.

Rinner, O., & Gegenfurtner, K. R. (2000). Time course of chromatic adaptation for color appearance and discrimination. *Vision Research*, *40*, 1813–1826.

Rovamo, J., Luntinen, O., & Näsänen, R. (1993). Modelling the dependence of contrast sensitivity on grating area and spatial frequency. *Vision Research*, *33*, 2773–2788.

Savoy, R. L., & McCann, J. J. (1975). Visibility of low-spatial-frequency sine-wave targets: Dependence on number of cycles. *Journal of the Optical Society of America*, *65*(3), 343–350.

Van der Horst, G. J. C., & Bouman, M. A. (1969). Spatio-temporal chromaticity discrimination. *Journal of the Optical Society of America*, *59*, 1482–1488.

Van Meeteren, A., & Vos, J. J. (1972). Resolution and contrast sensitivity at low luminance levels. *Vision Research*, *12*, 825–833.

Vogels, I. M. L. C., & Lambooij, M. (2014). Visibility of spatial chromatic contrast for lighting applications. In M. P. J. Aarts, I. Kalinauskaite, A. Haans, D. Lakens, L.M. Huiberts, Y. A. W. Kort, de, K. C. H. J. Smolders, A. Kuijsters, P. Khademagha, A. C. Schietecat, I. E. J. Heynderickx, M. G. M. Stokkermans, W. A. Ijsselsteijn, L. van Rijswijk, & F. Beute (Eds.), *Proceedings Experiencing Light 2014: International conference on the effects of light on wellbeing* (pp. 20–23). Eindhoven, The Netherlands.

Vos, J. J., & Walraven, P. L. (1972). An analytical description of the line element in the zone-fluctuation model of colour vision. I. Basic concepts. *Vision Research*, *12*, 1327–1344.

Watson, A. B. (2000). Visual detection of spatial contrast patterns: Evaluation of five simple models. *Optics Express*, *6*(1), 12–33.

Watson, A. B., & Yellott, J. I. (2012). A unified formula for light-adapted pupil size. *Journal of Vision*, *12*(10):12, 1–16, https://doi.org/10.1167/12.10.12. [PubMed] [Article]

Webster, M. A., De Valois, K. K., & Switkes, E. (1990). Orientation and spatial-frequency discrimination for luminance and chromatic gratings, *Journal of the Optical Society of America A*, *7*, 1034–1049.

Wuerger, S. M., Watson, A. B., & Ahumada, A. (2002). Towards a spatio-chromatic standard observer for detection. *Proceedings of the SPIE: Human Vision and Electronic Imaging VII*, *4662*, 159–172.